ORIGINAL ARTICLE

lajss.org
Latin American Journal of Solids and Structures

www.lajss.org

Analysis and optimization of impact energy absorption performance of mine refuge chamber filled with concave triangular negative poisson's ratio material

Kun Yang[a], Yiwen Chen[a]*, Yibo Wang[a], Hao Chen[a], Shourui Wang[a]

[a] Faculty of Mechanical Engineering and Automation, Liaoning University of Technology, Jinzhou, 121000, China. Email: yangkunwh@163.com, cccchenyiwen@163.com, 1399634566@qq.com, 1036629833@qq.com, 3164633386@qq.com

* Corresponding author

https://doi.org/10.1590/1679-78257438

Abstract

In this paper, negative poisson's ratio material is used to fill the interlayer of mine refuge chamber, and its characteristics such as light weight, thermal insulation, vibration isolation and impact resistance are used to improve the impact resistance and thermal insulation ability of mine refuge chamber. The equivalent density, elastic modulus and yield strength of negative poisson's ratio structure of material Q345 were obtained by simulation analysis. The negative poisson's ratio material was filled into the mine refuge chamber, and the impact energy absorption and explosion transient thermal analysis were carried out. The results show that compared with the prototype, the maximum inner skin temperature of the negative poisson's ratio refuge chamber is reduced by 44.86%, the transverse and longitudinal stiffeners temperature is reduced by nearly 46.77%, and the impact deformation is reduced by 35mm, which has better safety performance. The response surface optimization method was used to optimize the whole refuge chamber filled with negative poisson's ratio material, which was more secure than before.

Keywords

Mine refuge chamber, Negative poisson's ratio material, Thermal insulation, Safety performance, Optimization objective

Graphical Abstract

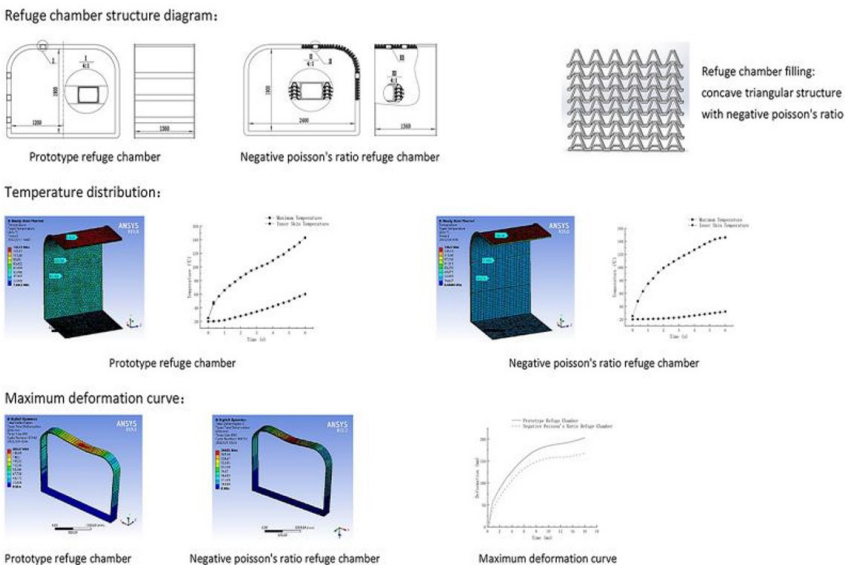

Received: January 10, 2023. In revised form: March 16, 2023. Accepted: March 17, 2023 Available online: March 24, 2023.
https://doi.org/10.1590/1679-78257438

1 INTRODUCTION

The project of “Mine Refuge Chamber” is listed as a sub-project of the special project of “Research and Development of Emergency Refuge Technology and Device for Employees in Distress” in China's 115th Key Science and Technology Support Plan. The purpose of research and development is developing various technologies for large-scale disaster emergency refuge for mining enterprises. It creates safe, reliable and guaranteed living space for mining enterprises in catastrophe environment and minimizes casualties in major disasters, which provides technical guarantee for the safety of coal mine production in the whole country (Zujing Zhang et al., 2016). In today's society, due to the rapid development of technology, traditional metals have long been unable to meet the needs of different industries for special mechanical properties. The special mechanical properties of negative poisson's ratio metal structure, such as high strength, fatigue resistance, dimensional stability and light weight have more advantages than traditional material structure, which has attracted many scholars to study it.

Li et al. (2020) established a negative poisson's ratio space cell with four concave surfaces. They explored the buckling behavior of sandwich plates formed by this cell. Shokri Rad et al. (2014) spliced two orthogonal concave hexagons together to form a spatial negative poisson's ratio cell of porous materials, and studied the mechanical properties of the cell by energy method. Yang N et al. (2020) fabricated and tested a set of spatial negative poisson's ratio structures, and proved that the stronger the negative poisson's ratio was, the greater the specific energy absorption of the structure was. Qiao and Chen (2015) studied the in-plane impact response of double-arrow negative poisson's ratio structure theoretically and numerically, and found that the size of the concave angle of the structure played a decisive role in the collapse stress under static and low-speed impact conditions, while the concave angle had little effect on collapse stress under high speed impact. Wang et al. (2019) proposed a novel composite multicellular structure. The results of simulation and numerical simulation showed that the energy absorption performance of the negative poisson's ratio structure was better than that of the star-shaped structure and the double-arrow structure at different impact velocities, and the performance improvement was particularly obvious at low impact conditions. Zixing and Wenbo (2018) established a new honeycomb structure with negative poisson's ratio and studied the influence of rotation angle and impact velocity on its in-plane impact performance. Yang S et al. (2017) proposed a negative poisson's ratio structure with rectangular perforation, and the design of negative poisson's ratio metamaterials by using topology optimization method provided a new way for the optimal design of metamaterial structures.

Due to its unique thermodynamic characteristics, materials with negative poisson's ratio have advantages such as excellent energy consumption, absorption and lightweight, etc. Therefore, they have a huge application prospect in the fields of medical equipment, protective equipment, aviation, navigation and national defense engineering (Dejan Tomažinčič et al., 2020). In this paper, the negative poisson's ratio material is filled into the sandwich structure of the negative poisson's ratio refuge chamber, and the heat insulation performance and impact resistance performance of the mine refuge chamber are studied. The response surface optimization method was adopted to optimize the maximum equivalent stress, acceleration and minimum deformation of the negative poisson's ratio filled mine refuge chamber. By changing the thickness of reinforcement bars, width of reinforcement bars, thickness of inner skin, thickness of outer skin and other design variables, the overall structure of mine refuge chamber filled with negative poisson's ratio material was optimized. Through multi-objective optimization, the impact resistance, safety and heat insulation performance of the chamber body are further improved, so as to protect the lives of coal miners who may be injured in coal mine accidents. Therefore, the research and optimization of negative poisson's ratio refuge chamber performance is of great significance to improve the quality of emergency refuge in coal mine industry.

2 ANALYSIS OF MECHANICAL PROPERTIES OF CONCAVE TRIANGULAR MATERIALS WITH NEGATIVE POISSON'S RATIO

The special mechanical properties of negative poisson's ratio materials are mainly due to the structural deformation in the micro units. Therefore, unlike traditional materials, the mechanical properties only depend on the properties of the base materials. The deformation mode of micro elements and the base material of negative poisson's ratio materials have important influence on the macroscopic mechanical properties of materials. Concave triangular structure with negative poisson's ratio has good stability and negative poisson's ratio effect (Jiang Y et al., 2018), and the structure is simple and easy to design and manufacture. Therefore, concave triangular negative poisson's ratio structure is chosen as the main research object in this paper.

2.1 Mechanical model of concave triangular structure with negative poisson's ratio

In order to study the static characteristics of negative poisson's ratio structure, the finite element model of a 6×8 multi-cell structure with a length of 80.8mm, a width of 5mm and a height of 49.6mm is established by SolidWorks in this

paper, as shown in Figure 1. Figure 1 shows the concave triangular cell with negative poisson's ratio structure. In the design process, the monocell is designed as a symmetrical structure, which is suitable for stable structure and uniform force. Its important components: L_1 and L_2 are the length of long cell wall and short cell wall at the bottom respectively. D_1 and D_2 are the cell wall thickness of the top flank and bottom respectively. α is the angle between the short cell wall and the axis of symmetry. β is the angle between the cell wall and the axis of symmetry. W is the horizontal length at the bottom of the monocell. F is the downward force on the top of the vertical concave triangular. As shown in Figure 1, $\alpha>\beta$ and α must be less than 50° for cell structure to have a complete negative poisson's ratio effect. D_1 is thicker than D_2. When the vertical top downward force F is loaded, D_2 preferentially breaks. Then D_1=1.5mm, D_2=0.72mm, L_1=15mm, L_2=6.16mm, α=45°, β=24°, W=5.85mm.

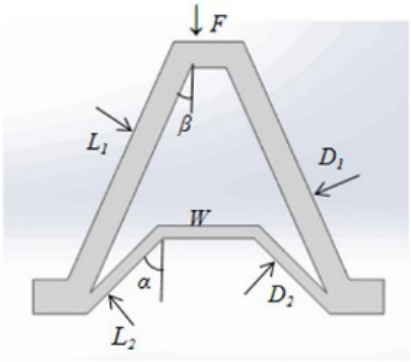

(a)Concave triangular cell with negative poisson's ratio structure

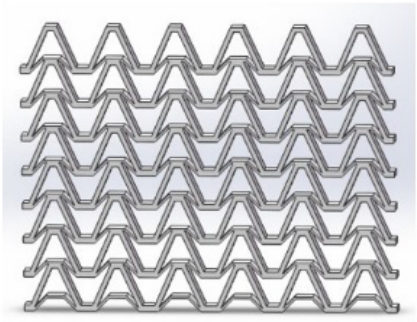

(b)Concave triangular structure with negative poisson's ratio

Figure 1 Concave triangular cell with negative poisson's ratio structure

2.2 Test and simulation of concave triangular quasi-static compression

2.2.1 Selection of experimental instruments and preparation of specimens for quasi-static compression

In the process of quasi-static compression test, due to the lack of 3D printing ability of metal materials, in order to verify the negative poisson's ratio effect and structural parameters of concave triangular structure, PLA material is used for 3D printing to obtain concave triangular structure for test to verify the accuracy of simulation results.

The concave triangular negative poisson's ratio structure specimens are prepared by melting deposition 3D printing. The specimen is a concave triangular multi-layer cell structure with negative poisson's ratio of 6×8. The base material is PLA polylactic acid. The in-plane quasi-static uniaxial compression test of concave triangular negative poisson's ratio structure is carried out by the SANS CMT5205 microcomputer controlled electronic universal testing machine. The test refers to the requirements of Test Method for flat compression Performance of Sandwich Structure or Core, and adopts the displacement loading method. The compression speed is set at 2mm/min, the total displacement is 36mm, and the maximum equivalent strain of the sample is about 40%. Concave triangular specimen and mechanical testing machine are shown in Figure 2.

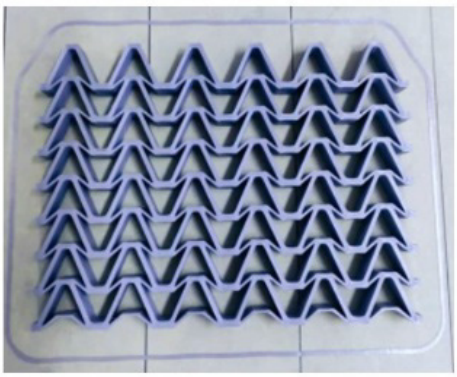

(a)Concave triangular specimen

(b)Mechanical testing machine

Figure 2 Concave triangular specimen and mechanical testing machine

2.2.2 Simulation analysis of concave triangular structure with negative poisson's ratio

The negative poisson's ratio structure model is imported into Ansys Workbench for quasi-static compression simulation. The material parameters of PLA are shown in Table 1. In this paper, tetrahedron-hexahedron mixed cell type was adopted, and the mesh size was set to 4.56mm after repeated verification. The solid cell model of divided mixed cells contains a total of 8790 nodes and 3398 cells. The test results of mesh sensitivity are as follows: Element quality is about 0.7, Aspect Ratio is 0.95, Jacobian Ratio is 0.92, Wraping Factor is 0.48, Orthogonal Quality is 0.95, it can be seen that the mesh quality is good.

Table 1 PLA material parameter table

Material	Density	Elastic Modulus	Tensile Strength	Poisson's Ratio	Tangent Modulus
PLA	1.20kg/dm^3	3000MPa	60MPa	0.3	1025MPa

PLA material is a renewable resource, has good biodegradability, is an excellent environmental protection material, and its fracture strength and initial modulus are small, has good ductility, and has been widely used in 3D printing tests. Zhao et al. (2020) tested the average young's modulus, poisson's ratio and tangent modulus of PLA materials through five groups of tests. Therefore, he selected Bilinear Isotropic Hardening plastic model. The tensile strength of PLA material was defined as 60MPa and the tangent modulus as 1025MPa. The stress-strain diagram of PLA material is shown in Figure 3.

A vertical downward displacement of -36mm was applied to the upper panel as a whole, and fixed constraints were added to all degrees of freedom except the two degrees of freedom in the horizontal direction on the bottom plane of the material with concave triangular negative poisson's ratio. So the model can move freely in the horizontal direction.

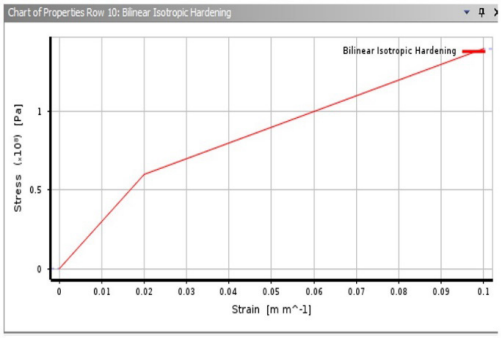

Figure 3 Stress-strain diagram of PLA material

2.2.3 Comparative analysis of quasi-static compression test and simulation

Through the comparison of quasi-static compression test and simulation analysis, it can be seen that the concave triangular structure with negative poisson's ratio has advantages such as light weight, heat insulation, vibration isolation and impact resistance. The negative poisson's ratio effect can be clearly seen from the second picture. The quasi-static compression process is divided into four stages: 6mm, 14mm, 24mm, 36mm. Test and simulation comparison of concave triangular quasi-static compression are shown in Figure 4.

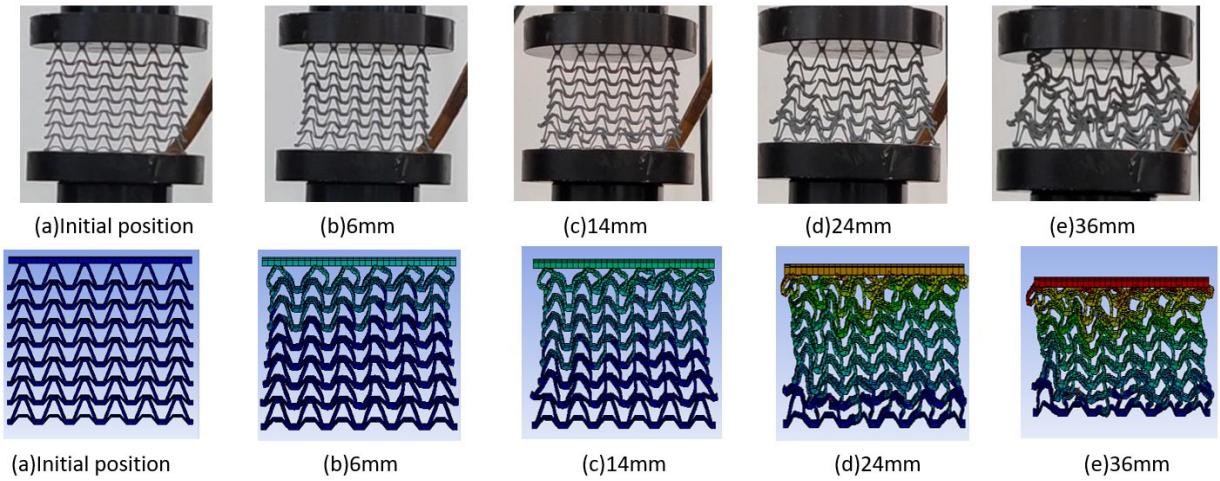

Figure 4 Test and simulation comparison of concave triangular quasi-static compression

Figure 5 shows test and simulation of pressure-displacement in concave triangular quasi-static compression. Under the action of load, the structure with negative poisson's ratio takes on elastic deformation. When the downward displacement is about 10mm, the simulated pressure gradually rises to the initial peak, and then the oscillation decreases. When the downward displacement is about 10mm, the experimental pressure gradually rises to the initial peak, and then begins to decrease, with a relatively stable reduction rate. By comparing the two curves, the average compressive load of the quasi-static simulation analysis is 1689N, and the average compressive load of the experimental analysis is 1834N, with an error of 7.9%. The initial pressure peak value of the quasi-static simulation analysis is 2641N, and that of the experimental analysis is 2359N, with an error of only 10.6%. The overall trend of the two curves is close to the experimental data. There are errors in the average crushing load and initial pressure peak, which is caused by the fact that PLA material is an idealized model in simulation, and no fracture occurred after the load is applied.

In Figure 5, the fluctuation of the curve indicates that the pressure changes greatly under this displacement, indicating that a certain layer has a crushing deformation. The greater the fluctuation, the greater the crushing deformation. However, with continuous pressure, several similar layers are stacked together after crushing, and other layers also have different degrees of plastic deformation, making the crushing deformation less violent, so the fluctuation is smaller and smaller.

In the test, a certain layer will first collapse and deform, and the materials in individual positions will fracture and be embedded in the cell holes, which will play a certain supporting role. With continuous pressure, the other layers also undergo plastic deformation of varying degrees (at this time not fracture). When adjacent layers collapse and pile on top

of each other, more material breaks off and becomes embedded in the hole. Therefore, there was no high level of pressure fluctuation at the later stage of the test, and the pressure kept increasing.

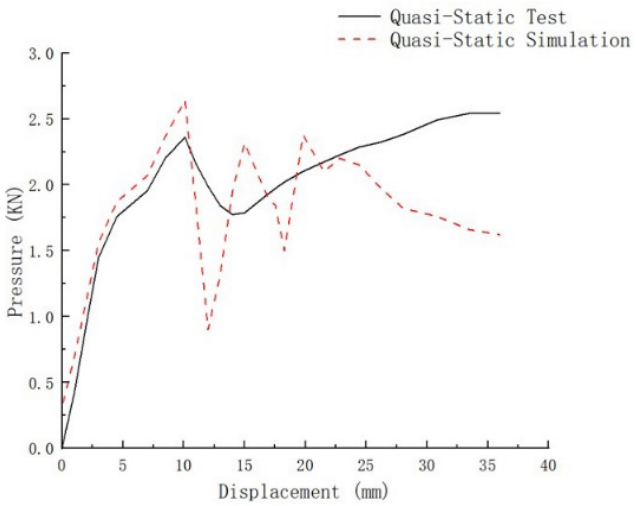

Figure 5 Test and simulation of pressure-displacement in concave triangular quasi-static compression

Figure 6 shows test and simulation of equivalent stress-strain in concave triangular quasi-static compression. As can be seen from the figure, the hydraulic test bench is under constant downward compression, and the structure gradually deforms. The reaction pressure measured by the test bench gradually increases, and the stiffness characteristics of the material also gradually increase due to the gradual increase in structural deformation. When the equivalent strain rate is less than 0.04, the simulation results are in good agreement with the experimental results. With the progress of the compression process, the equivalent stress of the simulation results is greater than the experimental results, because the ideal model of the simulation environment is that the material does not break and the whole structure can bear greater pressure. In conclusion, the error exists but does not affect the overall analysis. In the process of in-plane compression elastic deformation, the finite element simulation method is reliable and more efficient.

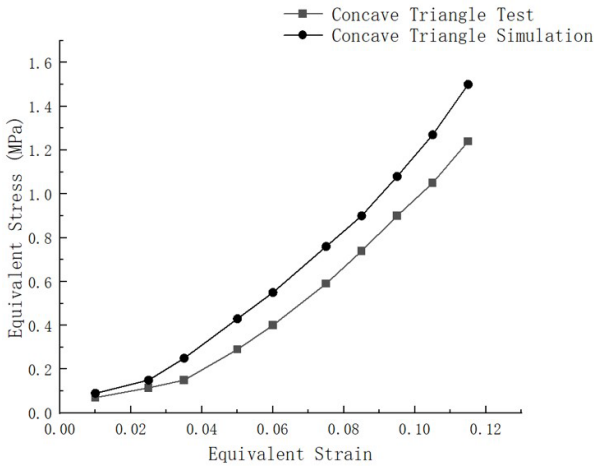

Figure 6 Test and simulation of equivalent stress-strain in concave triangular quasi-static compression

2.2.4 Compression simulation analysis of metal materials with negative poisson's ratio

The matrix material of traditional mine refuge chamber is Q345, so the matrix material of concave triangular negative poisson's ratio in mine refuge chamber is set as Q345. Through the simulation analysis of PLA material, the parameters of the negative poisson's ratio structure of Q345 matrix material are generalized, which prepares for the simulation analysis of the refuge chamber filling structure later. The density, elastic modulus and yield strength of Q345 are 7850kg/m^3, 206GPa and 345MPa respectively. Other parameters of Q345 are shown in Table 2.

Table 2 Q345 material parameter table

Material	Poisson's Ratio	Tensile Strength	Specific Heat Capacity	Thermal Conductivity	Coefficient of Linear Expansion
Q345	0.3	470-630MPa	460Jkg^{-1}K^{-1}	50Wm^{-1}K^{-1}	1.2×10^{-5}/K

By the method of equivalent mechanics, the stress-strain ratio of the structure in this direction under axial compression or tensile action is its equivalent elastic modulus, and the negative value of the ratio of transverse strain to axial strain under axial compression or tensile action is its equivalent poisson's ratio (Jacobs S et al., 2012). The equivalent stress-strain data obtained by simulation is brought into MATLAB, and its stress-strain curve is obtained as shown in Figure 7. Its equivalent elastic modulus E=29.537GPa is calculated.

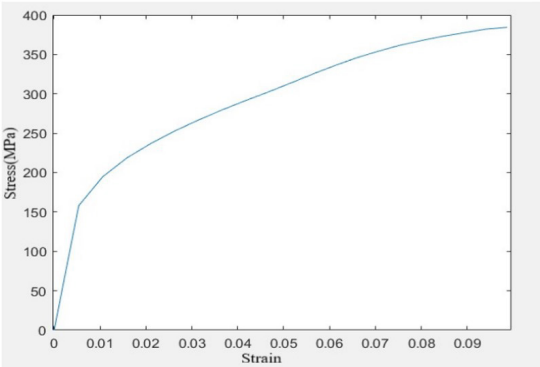

Figure 7 Quasi-static compressive stress-strain curve of Q345 material

When the structure with negative poisson's ratio is compressed, the structure collapses and absorbs energy, the density increases and the structure becomes more dense. Under the simulation environment, no local fracture occurs in the whole structure, and there is still an obvious negative poisson's ratio effect. The compression deformation process is shown in Figure 8.

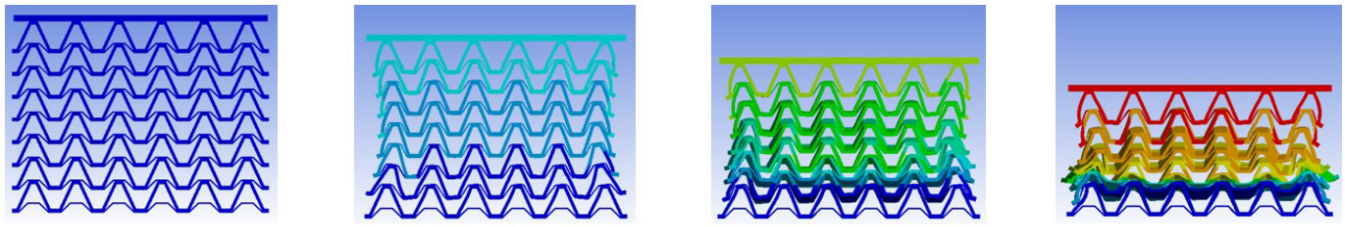

Figure 8 Quasi-static compression deformation diagram of Q345 material

The compression deformation process of Q345 material and PLA material is relatively similar, both have a compression trend in the horizontal and vertical directions, and the deformation conforms to the negative poisson's ratio effect. When the material is subjected to axial compression to form a negative strain, the transverse contraction will also form a negative strain. By measuring and calculating the model data after loading, the transverse strain of the concave triangular type is 0.0845, the axial strain is 0.233, and the equivalent poisson's ratio is -0.3633.

2.2.5 The equivalent density of concave triangular structure with negative poisson's ratio

The mechanical properties of negative poisson's ratio structure are different from those of traditional solid materials. The macroscopic properties of negative poisson's ratio structure are mainly determined by the shape and arrangement of matrix material and meso structure. Through the mechanical model of the length, thickness and angle between the sockets of the concave triangular cell in the negative poisson's ratio structure, the equivalent density of the material can be obtained according to the shape area parameter of the cell in the design process of the negative poisson's ratio structure, which provides guidance for the subsequent simulation analysis of the refuge chamber.

Assume that S_N is the area of the cell and S_M is the area of the matrix material in the cell. According to the definition of the equivalent density of the negative poisson's ratio structure, we can see:

$$\rho = \frac{S_M b \rho_M}{S_N b} \tag{1}$$

Where, it is assumed that the width of the long and short cell walls in the cell is the same, and b is the width of the cell walls in the cell. According to the cellular structure parameters in Figure 1, the relationship between S_N and S_M and the shape parameters of negative poisson's ratio structural units can be obtained respectively:

$$S_M = D_1(L_1 + W) + D_2(L_2 + W) \tag{2}$$

$$S_N = (L_1 sin\beta + W)(L_1 cos\beta - L_2 cos\alpha) \tag{3}$$

By substituting the concave triangular cell data into the formula, the equivalent density of material Q345 is obtained as: ρ =2805.4 kg/m^3.

3 STRUCTURAL DESIGN AND TRANSIENT THERMAL ANALYSIS OF MINE REFUGE CHAMBER FILLED WITH NEGATIVE POISSON'S RATIO MATERIAL

3.1 Structural design of refuge chamber filled with negative poisson's ratio material

The modeling should be consistent with the reality, and at the same time, various possible influencing factors should be considered to make appropriate simplification. In this paper, a certain type of refuge chamber is selected as the research object, the rated number of people is 4, and the internal size of the single section of the prototype mine refuge chamber is 2400×1360×1900mm, and the internal volume is about 6.20m^3. As shown in Figure 9, the chamber body is a closed structure, which is mainly welded by the chamber skin, stiffeners, flanges and other structures. The structure is relatively regular without complex curved surface. The inner and outer skin is made of Q345 structural steel with a thickness of 8mm, and the reinforcement is welded with 10# channel steel. The length×width is 100mm×96mm, the thickness is 5.3mm, and the radius of the top arc is 500mm. The inner size of the negative poisson's ratio refuge chamber is the same as that of the prototype. The skin and the negative poisson's ratio filling material are connected in the way of adhesive. The inner skin thickness is 3mm, the outer skin thickness is 5mm, and the reinforcement is welded with 5# channel steel, the length×width is 74mm×50mm and the thickness is 4.5mm. A 4-layer negative poisson's ratio structure with a height of 49.6mm is filled inside. According to the previous analysis results, the equivalent density, elastic modulus and poisson's ratio of the material with negative poisson's ratio are 2805.4kg/m^3, 29.537GPa and -0.3633 respectively.

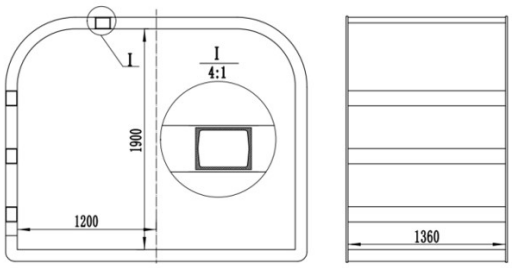

(a)Prototype refuge chamber

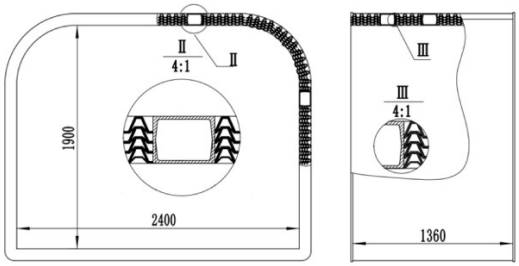

(b)Negative poisson's ratio refuge chamber

Figure 9 Refuge chamber structure diagram

3.2 Explosive transient thermal analysis of mine refuge chamber filled with negative poisson's ratio material

3.2.1 Finite element model for transient thermal analysis of refuge chamber explosion

In the finite element simulation analysis, the two kinds of refuge chambers were meshed using the mixed element type of tetrahedron-hexahedron, and the mesh size was set as 40mm. The mesh model of the prototype refuge chamber contains 101353 nodes and 46211 units. Due to the symmetry of the overall structure of the refuge chamber, only 1/4 of the model is analyzed to reduce the calculation amount, and symmetry constraints are imposed on the plane of symmetry. An ambient temperature of 22°C is applied to the inner surface of the refuge chamber, and a fixed constraint is added to the floor of the refuge chamber. The mesh model of the negative poisson's ratio material filled refuge chamber contains 117702 nodes and 46080 units. The matrix material of the refuge chamber is defined as Q345 steel. The thermal load and thermal boundary conditions applied to the negative poisson's ratio material filled refuge chamber are the same as those applied to the prototype refuge chamber.

The concave triangular structure negative poisson's ratio material with Q345 steel matrix is filled into the space between the reinforcement bars of the refuge chamber. The comparison between the prototype and the negative poisson's ratio refuge chamber is analyzed. According to the Interim Regulations On the Construction and Management of Underground Coal Mine Emergency Escape System, it is known that only the refuge chamber that can withstand 3s at 1200°C can meet the national standard (Fangfang Yan et al., 2012). Therefore, this paper analyzes the thermal performance of 6s in this high temperature environmentp. The transient temperature load of 1200°C is defined to be applied to the side plate and roof of the refuge chamber and the outside of the flange. The transient temperature load of 1200°C is defined to be applied to the side plate and roof of the refuge chamber and the outside of the flange. Meanwhile, the thermal conductivity of the air in the filling material is considered. The thermal conductivity is selected as the system default value. The Stagnant Air-Simplified Case boundary conditions are selected to apply the ambient temperature of 22°C on the inner surface of the refuge chamber, and add a fixed constraint to the bottom of the refuge chamber.

3.2.2 Analysis of simulation results

The transient thermal analysis of prototype refuge chamber model simulation is calculated and solved. The temperature cloud map of prototype refuge chamber and the temperature curve inside and outside the chamber body obtained by transient thermal analysis are shown in Figure 10. According to Figure 10(a), the maximum temperature of the prototype refuge chamber is 143.13°C, appears at the flange and top edge. The maximum outer skin temperature is about 137.80°C. The highest internal temperature of the skin is 60.26°C. The average temperature inside the skin is stable at about 47.996°C. According to the heating curve of prototype refuge chamber Figure 10(b), the maximum temperature of the prototype refuge chamber and the inner skin temperature rise rate are slightly different. The maximum temperature of the refuge chamber changes rapidly within 0 to 1.3s. The upward trend has since slowed slightly. The skin temperature in the refuge chamber changes slowly from 0 to 1.4s. Then it is gradually increased to 60.26°C.

The temperature cloud map and temperature curves of the material refuge chamber with negative poisson's ratio are shown in Figure 11. The maximum temperature of negative poisson's ratio is 146.40°C. Appears near the connection between the outer skin and the flange. The maximum temperature of the negative poisson's ratio is slightly higher than that of the prototype refuge chamber. That's because filling with negative poisson's ratio materials can effectively insulate heat. Heat is concentrated in the outer skin and flange junction. Because the external thermal load and thermal boundary conditions are completely consistent with the prototype refuge chamber conditions. According to the law of conservation of energy, the maximum temperature of the material chamber with negative poisson's ratio will be higher under the action of the same transient heat.

The temperature at the outer skin of the negative poisson's ratio material refuge chamber is about 142.36°C. The inner skin temperature is about 26°C. The temperature of internal transverse and longitudinal reinforcing bars is stable at about 31.99°C. The temperature of the transverse stiffeners at the connection between the inner arc transition and the side wall of the refuge chamber is stable at about 33.23°C. The temperature relative to the transverse and longitudinal stiffeners of the prototype refuge chamber decrease of nearly 46.77%. The maximum skin temperature of the new negative poisson's ratio material is 33.23°C. Compared with the prototype refuge chamber, the maximum inner skin temperature is reduced by 44.86%. It is proved that the negative poisson's ratio material refuge chamber has excellent heat insulation performance.

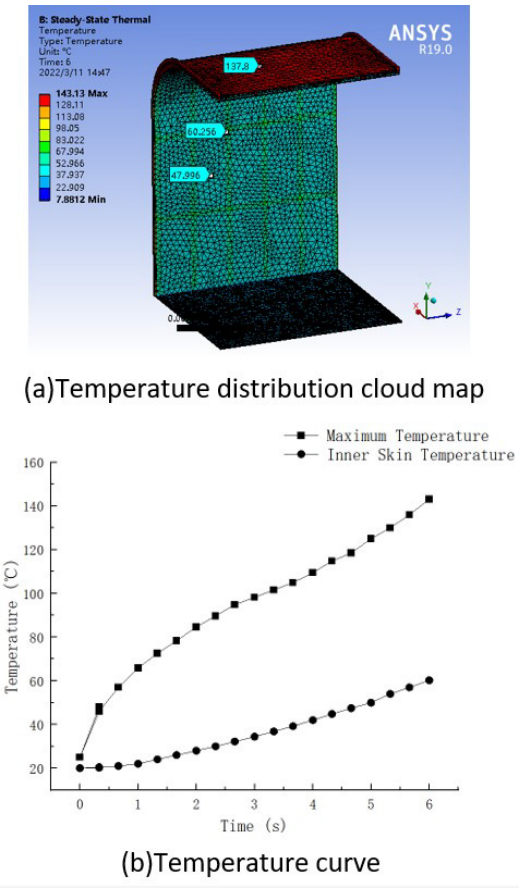

Figure 10 Temperature distribution of prototype refuge chamber

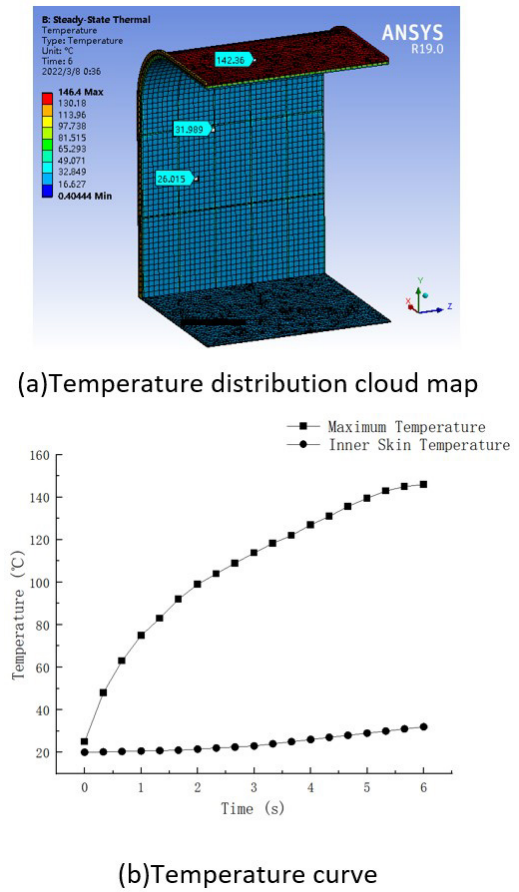

Figure 11 Temperature distribution of negative poisson ' s ratio material refuge chamber

4 IMPACT ENERGY ABSORPTION PERFORMANCE ANALYSIS OF MINE REFUGE CHAMBER FILLED WITH NEGATIVE POISSON'S RATIO MATERIAL

When the gas explods underground, the explosion process will create an ignition zone, a burning zone and a shock zone. Usually the flame expansion speed in the ignition area is about 6m/s. The instantaneous shock velocity in the combustion zone can reach 800m/s. But at about 100m before it spreads, the velocity of the shock wave will decay rapidly to about 70m/s. In the actual underground gas explosion environment, the impact of the stone splash on the chamber body is preferred to the occurrence of the positive pressure stage of the shock wave, so there is no high-temperature and high-pressure shock wave acting on the refuge chamber model during the collision. The ambient temperature of the simulation is set at 22°C, and the solution time is 15ms. In this paper, the collision speed is 100m/s, assuming that the rock is a sphere with a diameter of 200mm, and the impact collision between the simulated rock and the middle roof of the refuge chamber.

The base material of the refuge chamber is Q345, and the material properties remain unchanged. Johnson-Cook model is used to describe the strain rate effect of Q345, and the mixed tetrahedron-hexahedron mesh is divided. The mesh models of part of the refuge chamber are shown in Figure 12.

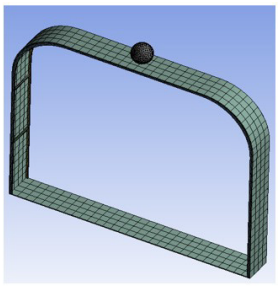

(a)Prototype refuge chamber

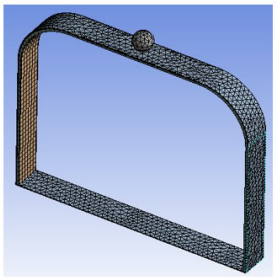

(b)Negative poisson's ratio refuge chamber

Figure 12 Mesh model of part of the refuge chamber

Johnson-Cook model was used to describe the strain rate effect of Q345.

$$\sigma_{yQ345} = \left(A + B\varepsilon_p^n\right)\left(1 + Cln\frac{\varepsilon}{\varepsilon_0}\right)\left[1 - \left(\frac{T - T_{room}}{T_{melt} - T_{room}}\right)^m\right] \tag{4}$$

Where, σ_{yQ345} is the dynamic yield strength, and A is the static yield strength, 374MPa. B is the hardening constant, 795.7MPa; n is hardening index, 0.45451; C is the strain rate strengthening parameter, 0.01586; m is the thermal softening index, 1.03; T_{room} is room temperature; The T_{melt} is 1400°C. The above parameters are related to Johnson-Cook model directly retrieved from the material library of Ansys Workbench.

At the same time, under conventional honeycomb material structure, the mechanical properties of negative poisson's ratio structure under impact load in a short period of time not only depend on the material properties of Q345 matrix, but also depend on the local collapse of structure caused by cell failure, and even the plastic deformation caused by local fracture. Therefore, geometric parameters of concave triangular cells have more significant influence on local stress distribution and strain variation trend.

The maximum equivalent stress curve of the two types of refuge chamber models is shown in Figure 13. According to the figure, in the initial stage of the collision between the ball and the chamber body, the maximum stress of the refuge chamber rapidly increases, reaching the maximum stress of 645.1MPa at 0.75ms, and then the maximum stress

of the chamber body gradually decreases and produces shock. Finally, 16ms later, the maximum stress of the prototype refuge chamber stabilizes at about 600MPa, and the maximum stress of the negative poisson's ratio refuge chamber stabilized at about 500MPa. Figure 14(a) shows the maximum equivalent stress cloud map of the prototype refuge chamber. It can be seen from the figure that at 8ms, the maximum stress of the refuge chamber appears at the contact position of the top of the refuge chamber, reaching 638.5MPa. The cloud map of the maximum equivalent stress of the negative poisson's ratio refuge chamber is shown in Figure 14(b). It can be seen from the figure that at 8ms, the maximum stress is 538.7MPa, which is the same as that of the prototype refuge chamber, but the maximum stress and the equivalent stress after final stabilization are smaller than that of the prototype refuge chamber.

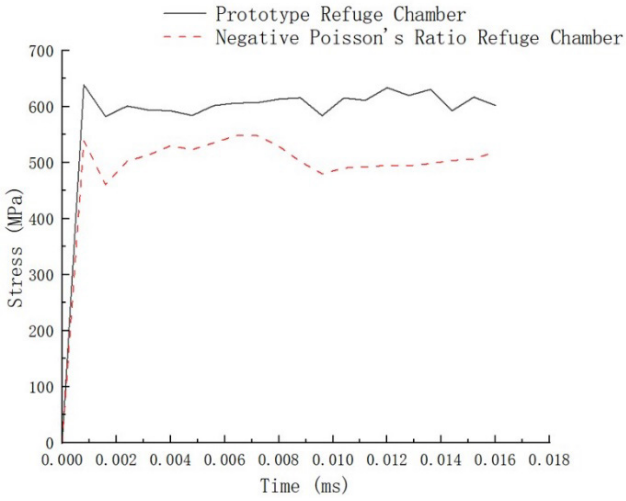

Figure 13 Maximum equivalent stress curve of mine refuge chamber

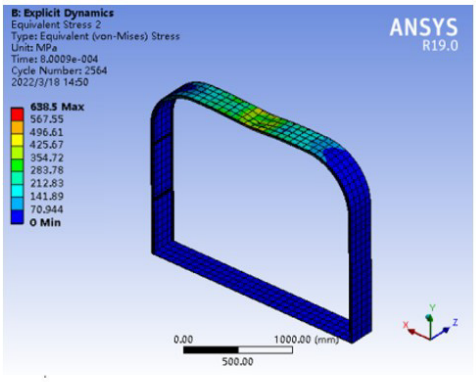

(a)Prototype refuge chamber

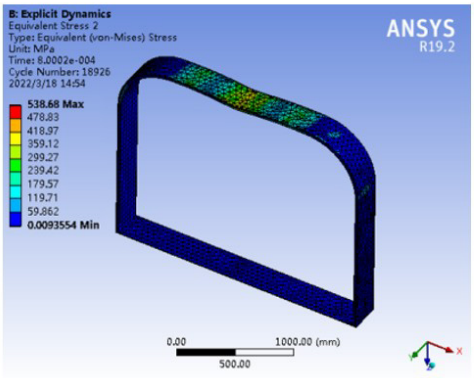

(b)Negative poisson's ratio refuge chamber

Figure 14 Maximum equivalent stress cloud map

The maximum deformation curves of the two types of refuge chamber over time are shown in Figure 15. According to the Figure 15, the deformation of the refuge chamber increased rapidly at the stage of 0 to 3.75ms, then the deformation rate of the refuge chamber begins to gradually decrease, and the overall deformation is still increasing. At 16ms, the maximum deformation of the two types of refuge chamber is 203mm and 168mm respectively. The maximum deformation cloud map of the two types of refuge chamber is shown in Figure 16. The contact position between the roof of the refuge chamber and the collider has been deeply dented, and it spreads outward along the collision center in the shape of water wave. The maximum deformation occurs at the central position of the top of the refuge chamber, namely the direct contact position of the collision. Other positions of the refuge chamber also have deformation, but compared with the top plate, the deformation in other positions is very small.

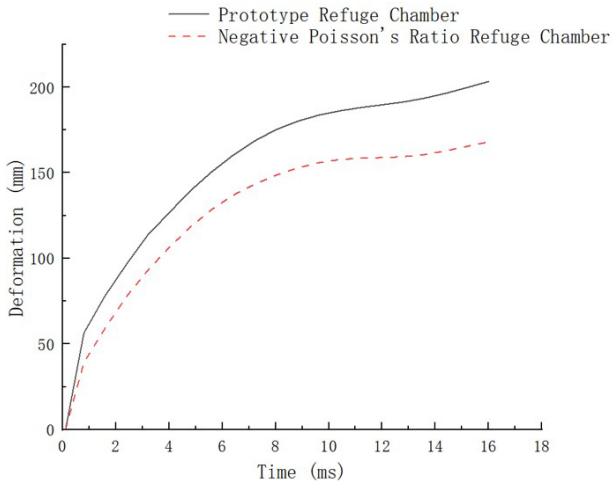

Figure 15 Maximum deformation curve of the refuge chamber

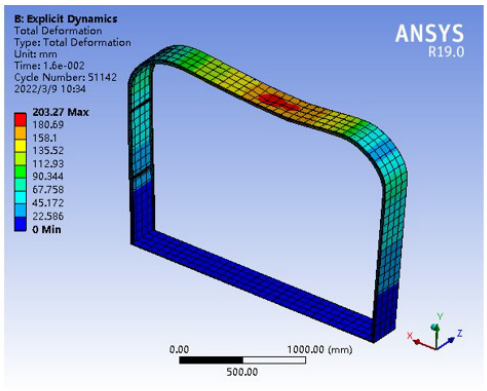

(a)Prototype refuge chamber

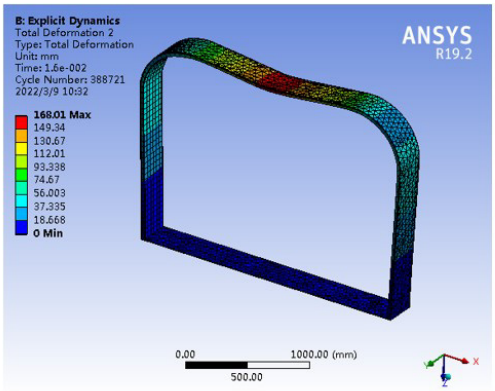

(b)Negative poisson's ratio refuge chamber

Figure 16 Maximum deformation cloud map

The acceleration curves of the two types of refuge chamber are shown in Figure 17. It can be seen from the figure that the prototype refuge chamber has the maximum acceleration of 4.687×10^8(m·s^{-2}) at 2.75ms, and then shows a fluctuation decreasing at 3ms to 15ms. The new negative poisson's ratio refuge chamber has a maximum acceleration of 2.186×10^8(m·s^{-2}) at 1.85ms, and then shows a fluctuation decreasing at 2ms to 15ms, and the amplitude and mean acceleration are smaller than those of the original refuge chamber.

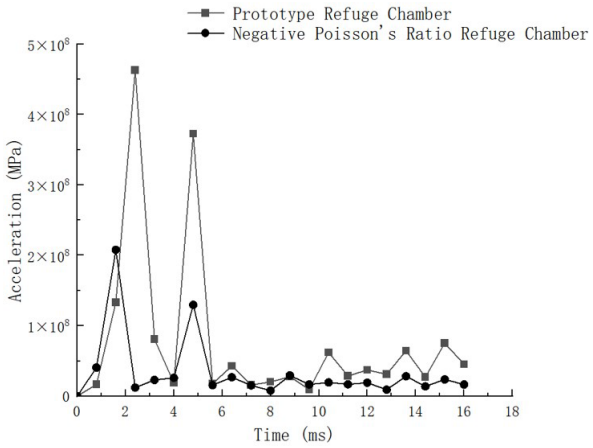

Figure 17 Acceleration curve of the refuge chamber

5 MULTI-OBJECTIVE OPTIMIZATION DESIGN OF MINE REFUGE CHAMBER FILLED WITH NEGATIVE POISSON'S RATIO MATERIAL

5.1 Multi-objective optimization mathematical model

By comparing the known negative poisson's ratio structure filled mine refuge chamber has better impact resistance and heat insulation performance than the prototype refuge chamber. When collision occurs, the refuge chamber deforms collapses and absorbs energy, and part of the energy is dissipated. The smaller the acceleration during collision, the longer the energy absorption time of the deformable structure of the refuge chamber, and the smaller the damage of the collider to the refuge chamber structure (Shuyi Yang et al., 2013). Therefore, the maximum equivalent stress, the minimum acceleration and the minimum deformation of the negative poisson's ratio filled mine refuge chamber are taken as the optimization objective. Under the condition that the strength of the refuge chamber is satisfied, the above three objective functions are optimized under the condition that the mass of the refuge chamber is not increased, and the three objectives are transformed into single objective optimization with equal weight and normalized processing. The optimization mathematical model is as follows:

$$minF(X)=\left[\alpha\frac{f_{1min}-f_1(X)}{f_{1max}-f_{1min}}+\alpha\frac{f_2(X)-f_{2min}}{f_{2max}-f_{2min}}+\alpha\frac{f_3(X)-f_{3min}}{f_{3max}-f_{3min}}\right] \tag{5}$$

$$\begin{cases} m(X)\approx[m] \\ X=[x_1,x_2,x_3,x_4]^T \\ 7\le x_1\le 9 \\ 20\le x_2\le 24 \\ 5\le x_3\le 7 \\ 18\le x_4\le 22 \end{cases} \tag{6}$$

In the formula: f_{1max} and f_{1min} are the maximum and minimum equivalent stress of the chamber respectively. f_{2max} and f_{2min} are the maximum and minimum deformation of the chamber respectively. f_{3max} and f_{3min} are the maximum and minimum acceleration of the chamber under impact. $m(X)$ and $[m]$ are the mass of the negative poisson's ratio refuge chamber before and after optimization. α=1/3 represents the same proportion of each objective function.

5.2 Parametric design of dimension variables

The thickness of outer skin, thickness of sandwich plate with negative poisson's ratio, width of reinforcement bars and size parameters of reinforcement bars are set as input variables for P1, P2, P3 and P4, and the weight of P5 chamber

body is restricted within 245kg~255kg. P6, P7 and P8 are designed with the minimum maximum equivalent stress, minimum collision acceleration and minimum hull deformation of the negative poisson's ratio filled mine refuge chamber as the design objectives. The design variables and variable variation range of negative poisson's ratio refuge chamber are shown in Table 3. The design optimization objectives of negative poisson's ratio refuge chamber are shown in Table 4.

Table 3 Design variable parameters

Design Variables	Variables Name	Size Initial Value	Change Scope
P1	Skin thickness outside cabin/mm	8	7~9
P2	Negative poisson's ratio interlayer thickness/mm	22	20~24
P3	Stiffener width/mm	6	5~7
P4	Rib thickness/mm	20	18~22

Table 4 Optimization target item table

Design Variables	Variables Name	Original Design Scheme Value
P6	Maximum equivalent stress/MPa	519.64
P7	Maximum acceleration/(mm*s^-2)	1.653×10^{7}
P8	Maximum deflection/mm	168.01

In this paper, DOE, an experimental design based on response surface optimization, and CCD, a central composite design method, were adopted as the sample type to generate 24 experimental design points. The results of each design point are shown in Table 5.

Table 5 Partial design point data

	1	2	3	...	11	12	...	23	24
P1	7	9	8	...	7.295	8.704	...	7.296	8.7042
P2	22	22	20	...	20.592	23.408	...	23.408	23.41
P3	6	6	6	...	6.7042	5.296	...	6.704	6.704
P4	20	20	20	...	20	18.592	...	21.408	21.408
P5	253.27	253.27	253.27	...	253.27	253.27	...	253.27	253.27
P6	518.76	521.32	520.73	...	520.66	458.7	...	518.67	518.61
P7	2.17×10^{7}	1.66×10^{7}	2.65×10^{7}	...	1.74×10^{7}	3.85×10^{7}	...	2.06×10^{7}	1.95×10^{7}
P8	167.99	167.71	168.11	...	167.82	167.48	...	168.09	168.1

5.3 Response surface optimization based on genetic iteration method

In the multi-objective optimization analysis, due to the large number of design variables and objective functions, it is often impossible to achieve the optimal solution satisfying all conditions. Only through the design structure analysis can several candidate schemes of the optimal design based on the objective optimization be generated. The results of candidate schemes are shown in Table 6.

Table 6 Candidate point data

Variable Name	Candidate Point 1	Candidate Point 2	Candidate Point 3
P1/mm	8.7703	8.7703	8.8538
P2/mm	20.683	20.224	21.41
P3/mm	5.2868	5.2868	5.6112
P4/mm	18.532	18.516	18.851
P5/kg	249.36	248.59	256.93
P6/Mpa	473.96	477	494.06
P7/(mm*s^-2)	2.6844×10^{7}	2.6211×10^{7}	2.3609×10^{7}
P8/mm	166.43	166.55	167.4

Star comparison is made between the candidate point schemes, and candidate point 1 is selected as the optimized new design point. Considering the actual processing process, the data are rounded and the thickness of outer skin is 9mm, the thickness of negative poisson's ratio refuge chamber body is 21mm, the width of reinforcing bars is 5mm, and the thickness of reinforcing bars is 19mm.

Build the analysis project in Ansys Workbench, set the size parameters and constraints, determine the optimization area, and select the optimal scheme according to the model star rating. The response surface model is constructed, and the genetic iterative method is adopted for response surface analysis (She Zi Hang, 2022). The fitting accuracy of the optimized results is shown in Figure 18. The determination coefficient of each output target can reach more than 0.99, and the overall system parameters have the best fitting effect. Part of the 3D response surface are shown in Figure 19.

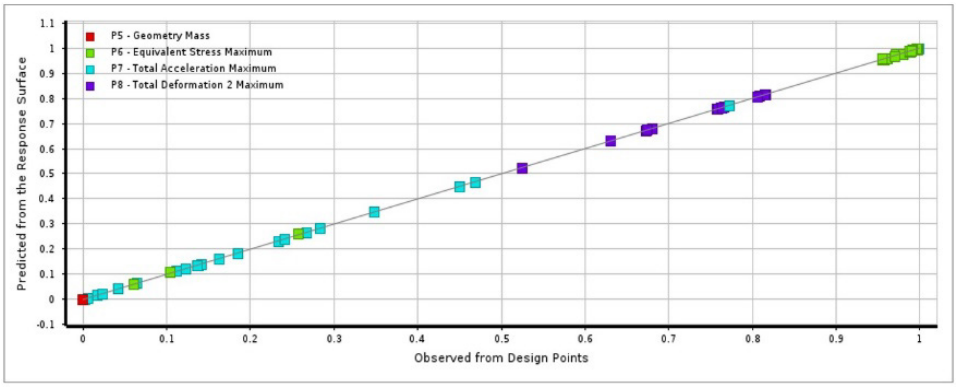

Figure 18 Response surface fitting accuracy

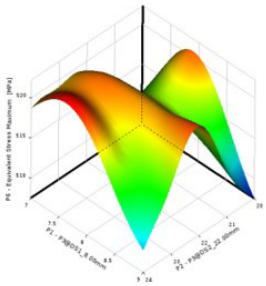

(a)P1 P2 P6 3D Response Surface

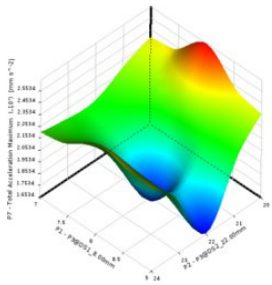

(b)P1 P2 P7 3D Response Surface

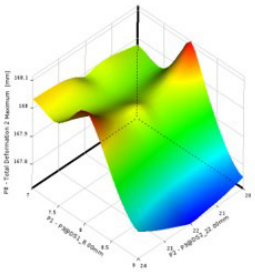

(c)P1 P2 P8 3D Response Surface

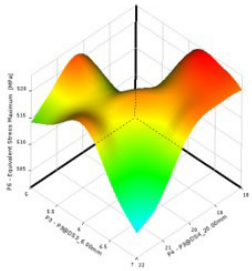

(d)P3 P4 P6 3D Response Surface

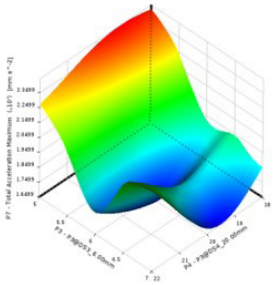

(e)P3 P4 P7 3D Response Surface

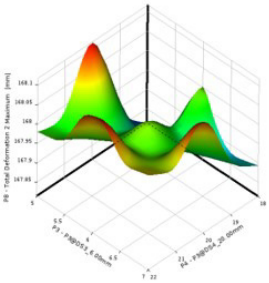

(f)P3 P4 P8 3D Response Surface

Figure 19 Response Surface Cloud Map

5.4 Simulation analysis of the optimized negative poisson's ratio refuge chamber

The optimized model is imported into Workbench for simulation, and the obtained equivalent stress cloud map and deformation cloud map of the 16ms refuge chamber after collision are shown in Figure 20 and Figure 21.

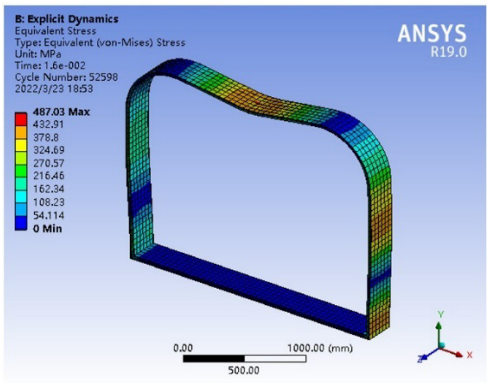

Figure 20 Equivalent stress cloud map

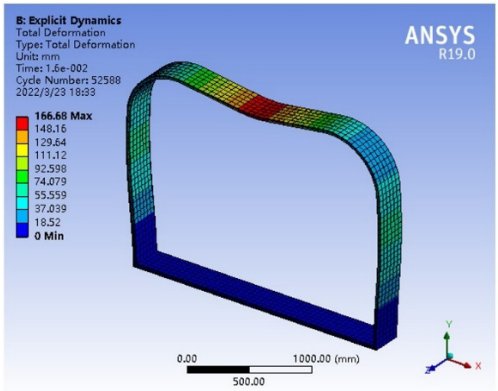

Figure 21 Deformation cloud map

The optimized front chamber mass is 253kg. The optimized chamber mass is 251kg. The maximum equivalent stress of the optimized negative poisson's ratio refuge chamber is 487.03MPa and 32.61MPa smaller than that before optimization. The maximum deformation cloud map is 166.68 mm. It is 1.33 mm smaller than that before optimization. The mean acceleration is 2.72×10^{7} (mm*s^-2). It is slightly higher than that before optimization. Under the condition of meeting the actual working conditions, the production of the parts of the refuge chamber is more convenient and the practical safety is increased.

6 CONCLUSION

In this paper, the concave triangular negative poisson's ratio structure is used as the sandwich material to fill the chamber body structure of a certain type of mine refuge chamber by taking advantage of its lightweight characteristics and special mechanical properties. The internal concave triangular negative poisson's ratio structure is simulated and analyzed, and its equivalent density, equivalent elastic modulus and equivalent poisson's ratio are calculated. It is proved that concave triangular structure has obvious negative poisson's ratio effect. The results of transient thermal analysis, quasi-static compression test, structural design and safety analysis show that the negative poisson's ratio mine refuge chamber has better performance than the prototype in acceleration, stress, maximum temperature and other aspects. The results are as follows:

(1) Heat insulation: Compared with the prototype, the maximum inner skin temperature of the negative poisson's ratio material refuge chamber is reduced by 44.86%, and the temperature at the transverse and longitudinal stiffening bars is reduced by nearly 46.77%, which proves that the negative poisson's ratio material refuge chamber has excellent heat insulation performance.

(2) Impact: The maximum stress of the negative poisson's ratio refuge chamber is stable at about 500MPa, which is lower than that of the prototype refuge chamber. The maximum deformation of the negative poisson's ratio refuge chamber is 168mm, which is less than 203mm of the prototype refuge chamber. The maximum acceleration of the

material chamber with negative poisson's ratio is $2.186\times10^{8}/(m\cdot s^{-2})$, which is smaller than that of the prototype refuge chamber $4.687\times10^{8}/(m\cdot s^{-2})$, and then the fluctuation decreases, and the amplitude and mean acceleration are smaller than that of the prototype refuge chamber.

(3) Optimization: A multi-objective optimization design is carried out for the maximum absorbed total energy and minimum acceleration and deformation of the negative poisson's ratio filled mine refuge chamber. According to the simulation analysis, the maximum equivalent stress of the optimized refuge chamber is reduced by 32MPa and the impact deformation of the refuge chamber body is reduced by 35mm, which proves that the optimized negative poisson's ratio of the refuge chamber is safer than that before optimization.

Author's Contributions: Conceptualization, Kun Yang and Yiwen Chen; Methodology, Kun Yang and Yiwen Chen; Investigation, Kun Yang, Yiwen Chen, Yibo Wang, Hao Chen and Shourui Wang; Writing - original draft, Kun Yang and Yiwen Chen; Writing - review & editing, Kun Yang, Yiwen Chen, Yibo Wang, Hao Chen and Shourui Wang; Funding acquisition, Kun Yang, Yiwen Chen, Yibo Wang, Hao Chen and Shourui Wang; Resources, Kun Yang, Yiwen Chen, Yibo Wang, Hao Chen and Shourui Wang; Supervision, Kun Yang.

Editor: Marcílio Alves

References

Zujing Zhang, Yanping Yuan, Kequan Wang, Xiangkui Gao, Xiaoling Cao. (2016). Experimental investigation on Influencing Factors of air curtain systems barrier efficiency for mine refuge chamber[J]. Process Safety and Environmental Protection 102:48-56.

Li C, Shen H S, Wang H. (2020). Postbuckling behavior of sandwich plates with functionally graded auxetic 3D lattice core[J]. Composite Structures 237(C):118-124.

Shokri Rad M, Prawoto Y, Ahmad Z. (2014). Analytical solution and finite element approach to the 3D re-entrant structures of auxetic materials[J]. Mechanics of Materials 74:76-87.

Yang N, Deng Y, Mao Z, et al. (2020). Cross-like lattices with tailorable mechanical properties[J]. Materials Letters 128-130.

Qiao J X, Chen C Q. (2015). Impact resistance of uniform and functionally graded auxetic double arrowhead honeycombs[J]. International Journal of Impact Engineering 83(9):47-58.

Wang H, Lu Z X, Yang Z Y, et al. (2019). In-plane dynamic crushing behaviors of a novel auxetic honeycomb with two plateau stress regions[J]. International Journal of Mechanical Sciences 151(2):746-759.

LU Zixing, WU Wenbo. (2018). Numerical simulations for the in-plane dynamic crushing of honeycomb material with negative Poisson's ratio based on rotating triangle model[J]. Acta Armamentarii 39(1):153-160.

Yang S, Chalivendra V B, Kim Y K. (2017). Fracture and impact characterization of novel auxetic Kevlar®/Epoxy laminated composites[J]. Composite Structures 168:120-129.

Dejan Tomažinčič, Matej Vesenjak, Jernej Klemenc. (2020). Prediction of static and low-cycle durability of porous cellular structures with positive and negative Poisson's ratios[J]. Theoretical and Applied Fracture Mechanics 106(C): 147-160.

Jiang Y, Liu Z, Matsuhisa N. (2018). Auxetic mechanical metal materials to enhance sensitivity of stretchable strain sensors[J]. Advanced Materials 30(12):235-245.

Jian Zhao, Xiaopeng Liu, Zewu Wang. (2020). Research on mechanical properties of PLA materials based on 3D printing [J]. Plastic Industry 48(7):139-143.

Jacobs S, Coconnier C, DiMaio D. (2012). Deployable auxetic shape memory alloy cellular antenna demonstrator, Design, manufacturing and modal testing[J]. Smart Materials and Structures 21(7):75-93.

Fangfang Yan, Xiaodong Xu. (2012). Application of negative Poisson's ratio flexible honeycomb structure in variant wing[J]. China Mechanical Engineering 23(5):542-546.

Shuyi Yang, Jingjing Li, Yaobin Sun. (2013). Mine rescue capsule dynamics modeling and stress analysis[J]. The 6th International symposium on precision mechanical measurement, Guiyang, China 8916:719-728.

She Zi Hang. (2022). A Class of Unconditioned Stable 4-Point WSGD Schemes and Fast Iteration Methods for Space Fractional Diffusion Equations[J]. Journal of Scientific Computing 92(1): 238-249.